Available online at www.sciencedirect.com
SCIENCE DIRECT
Journal of Catalysis 227 (2004) 384–397
JOURNAL OF CATALYSIS
www.elsevier.com/locate/jcat

On the nature of different iron sites and their catalytic role in Fe-ZSM-5 $DeNO_x$ catalysts: new insights by a combined EPR and UV/VIS spectroscopic approach

M. Santhosh Kumar [a], M. Schwidder [b], W. Grünert [b], A. Brückner [a,*]

[a] *Institut für Angewandte Chemie Berlin-Adlershof e. V., Richard-Willstätter-Str. 12, D-12489 Berlin, Germany*
[b] *Lehrstuhl für Technische Chemie, Ruhr-Universität Bochum, D-44780 Bochum, Germany*

Received 28 April 2004; revised 6 July 2004; accepted 4 August 2004

Available online 3 September 2004

Abstract

Fe-ZSM-5 $DeNO_x$ catalysts prepared from H-ZSM-5 by different ion-exchange procedures have been analyzed by EPR and UV/VIS diffuse reflectance spectroscopy (DRS) ex situ after synthesis, calcination, and use in catalysis as well as in situ during calcination. The results have been correlated with the catalytic behavior of these materials in the selective catalytic reduction (SCR) of NO by isobutane or ammonia. In comparison to previous studies of the same samples by XAFS, XRD, XPS, TPR, and Mössbauer spectroscopy, the combination of EPR and UV/VIS-DRS was more sensitive for distinguishing between different types of isolated Fe species as well as Fe_xO_y aggregates of different size (oligonuclear clusters or large particles). It was found that aggregated species are formed at the expense of mononuclear Fe sites upon calcination at 873 K, and that aggregate formation is slightly favored by calcination with higher heating rates as well as by high Si/Al ratios of the parent H-ZSM-5. Use in SCR of NO leads to further growth and restructuring of Fe_xO_y clusters. From the comparison of structural and catalytic properties of different Fe-ZSM-5 catalysts it can be concluded that the SCR of NO by NH_3 is catalyzed by different entities (mononuclear Fe sites, Fe_xO_y oligomers, surface of iron oxide particles). The results suggest that mononuclear Fe sites are also involved in the SCR with isobutane. Clustered sites, which may contribute to SCR with isobutane as well, appear to cause nonselective oxidation of the reductant (isobutane or ammonia) at higher temperatures.

Keywords: EPR; UV/VIS-DRS; Fe-ZSM-5 $DeNO_x$ catalysts; Fe^{3+} single sites; Iron oxide clusters

1. Introduction

In recent years, MFI-type zeolites containing nonframework iron species, such as Fe-ZSM-5, have been recognized as highly efficient catalysts for a number of reactions, e.g., selective oxidation of benzene to phenol [1,2], N_2O decomposition [3], and selective catalytic reduction (SCR) of NO_x by NH_3 [4] and hydrocarbons [5,6]. In the preparation of Fe-ZSM-5 catalysts, traditional aqueous exchange techniques aiming at the replacement of H^+ or Na^+ cations of the ZSM-5 matrix by Fe^{2+} or Fe^{3+} ions are nowadays largely disregarded despite reports of considerable achievements with special techniques [5,7,8], because they most likely involve iron oxo- or hydroxo cations that can undergo complex chemical transformation during subsequent calcination and are believed to lead to highly heterogeneous materials with poor reproducibility. Instead, attention was focused on overexchanged Fe-ZSM-5 obtained by chemical vapor deposition (CVD) of $FeCl_3$ into the pores of H-ZSM-5 followed by subsequent washing and calcination steps [5]. The material was prepared by many groups, which reported high and reproducible NO reduction activities with the reductant isobutane [5,9–11], but also outstanding activities with the reductant ammonia [4,12,13].

* Corresponding author. Institut für Angewandte Chemie Berlin-Adlershof e. V., PO Box 96 11 56, D-12474 Berlin. Fax: +49 30 6392 4454.
E-mail address: brueckner@aca-berlin.de (A. Brückner).

0021-9517/$ – see front matter
doi:10.1016/j.jcat.2004.08.003

In this preparation, zeolite Brønsted sites are completely consumed in the CVD step but reappear partly after calcination. Together with a recourse on enzymatic models, this has inspired the view that the active sites responsible for the high SCR activities are binuclear intrazeolite Fe oxo complexes, which has been supported by several EXAFS investigations [14–17]. Other groups concluded from their characterization studies that their Fe-ZSM-5 samples, which exhibited comparable SCR activities, contain a multitude of Fe species, among them isolated sites, clusters of a wide range of nuclearities and large oxide aggregates [10,11]. Therefore, alternative suggestions about the active site structure of Fe-ZSM-5 SCR catalysts have been also made. They include Fe_4O_4 clusters [18], isolated mononuclear sites [19], or all oligomeric clusters with low nuclearities including mononuclear sites [10,20]. Large oxide particles are believed to be rather inactive [10,21].

The heterogeneity of the Fe site structure in Fe-ZSM-5 prepared via the CVD method has been suggested on the basis of a multitechnique study comprising XRD, EXAFS, Mössbauer spectroscopy, TPR, FTIR, and XPS [10]. In this study, the preparation was applied to parent zeolites of different Si/Al ratio, and different washing and calcination protocols were used to create catalysts with a different degree of site isolation. A sample made by solid-state ion exchange (SSIE), which contained large Fe_2O_3 aggregates outside the pores along with other Fe species, was also included as well as a material prepared by a novel mechanochemical route, which, based on EXAFS results, was believed to contain exclusively Fe^{3+} single sites [20]. It turned out, however, that a reliable identification of the different Fe species coexisting in these materials and, in particular, their relative quantities, is not straightforward because the sensitivity of the techniques for the various types of Fe species differs. Thus, it was found that EXAFS is most sensitive for highly disperse Fe sites while the scattering contribution from higher shells, which is expected to indicate the presence of Fe_xO_y clusters, was near the detection limit or hardly significant for all samples except the one prepared by SSIE, in which crystalline, probably extrazeolite α-Fe_2O_3 was also detected by XRD. In contrast, Mössbauer and TPR measurements indicated a much larger degree of clustering than was found by EXAFS. A major goal of the present study is to clarify these contradictions and to give more insight into the structures of Fe oxo sites formed by the preparations typically employed in the literature, in particular the CVD technique. This was achieved by the use of additional techniques which are able to distinguish between isolated Fe species of different structures on the one hand and between Fe_xO_y clusters of different nuclearity on the other hand. EPR first of all and also UV/VIS spectroscopy are suitable techniques for this purpose.

EPR spectroscopy is a powerful tool for identifying isolated Fe^{3+} species of different coordination geometries by the position of their signals [2,8,21–25] as well as Fe_xO_y cluster species of different degrees of aggregation by analysis of the mutual magnetic interactions of the Fe sites [26]. UV/VIS spectroscopy, on the other hand, is especially sensitive to charge-transfer (CT) bands of Fe^{3+}, the wavelength of which depends on the coordination number and the degree of aggregation [27]. We have therefore reexamined the samples studied in [10] and [20] by these methods with the aim to better differentiate the Fe sites present and to detect changes in their structure caused by different preparation conditions (mode of Fe introduction, Si/Al ratio of the parent H-ZSM-5, calcination, and washing protocols) and by use in the SCR of NO_x than it was possible with the methods used in the previous study. It will be confirmed that Fe-ZSM-5 catalysts with high Fe content—even if prepared by the CVD technique—contain iron in a wide variety of species. While this is an unfavorable situation for identifying active sites for any reaction, it will be shown that the qualitative trends in the structural and catalytic data obtained support the view that mononuclear Fe ions are involved in the SCR of NO by isobutane and by ammonia. A study with catalysts prepared by a technique that allows highly disperse Fe sites with a better control of site distribution to be produced will be presented in the near future.

2. Experimental

The preparation of the samples has been described in detail in [10,20]. Therefore, only a brief summary will be given here, and the sample code used to label the samples with reference to the preparation details will be explained. Two ZSM-5 materials with different Si/Al ratios (≈ 14 and ≈ 40, the latter with high density of structure defects, e.g., silanol nests, labeled A and B, respectively) have been employed. The first one (A) was used with all preparations, the other one only for comparative purposes. Fe ions have been introduced into the parent H-ZSM-5 matrices by three different methods: (i) Chemical vapor deposition using anhydrous $FeCl_3$ followed by washing with 1 or 10 L water per 5 g catalyst (W1 and W10, respectively) and calcination in air at 873 K with heating rates of 0.5 or 5 K/min (C0.5 and C5, respectively), (ii) solid-state ion exchange with $FeCl_3 \times 6H_2O$—different from the procedure outlined in [10] *with* subsequent washing, which leads to a significant decrease of the iron content in the case of the SSIE preparation, and (iii) treatment by a mechanochemical route (MR) that implies intense grinding of the parent H-ZSM-5 with $FeCl_3 \times 6H_2O$, followed by 2–3 short-time washing steps (0.5 L water per 2 g catalyst). This material was studied in the present work starting from the uncalcined state, while the usual calcination conditions were 873 K, air, 1 h as with the other materials [20].

The label is composed of the symbols for the ZSM-5 type, Fe introduction route, washing intensity, and heating rate during calcination. Thus, A(CVD, W1, C0.5) means a material in which Fe was introduced via CVD into ZSM-5 of type A, washed with 1 L water per 5 g catalyst, and

calcined with a heating rate of 0.5 K/min. Missing symbols mean that the corresponding step has been omitted (i.e., A(CVD, W1) is A(CVD, W1, Cx) before calcination with a ramp of x K/min). The Fe content of the samples determined from the X-ray absorption step height in the XAFS spectra ([10,20], validated by ICP analyses of selected samples), amounted to 0.5 wt% for A(MR), 5.4 wt% for A(CVD, W1), 5.0 wt% for A(CVD, W10), 5.2 wt% for A(SSIE, W1), and 2.6 wt% for B(CVD, W1). It has been recently reported that the introduction of iron via $FeCl_3$ may plug pores in the parent ZSM-5 [28]. Indeed, in our samples the pore volume of the parent H-ZSM-5 zeolite decreased from 0.15 to 0.105 cm^3/g for A(CVD, W1, C5), A(CVD, W10, C5), and, surprisingly, A(MR, C5), while the pore volume of B(CVD,W1, C5) was 0.084 cm^3/g, and that of A(SSIE, W1, C5) 0.064 cm^3/g.

UV/VIS-DRS measurements were performed with a Cary 400 spectrometer (Varian) equipped with a diffuse reflectance accessory (praying mantis, Harrick). To reduce light absorption, samples were diluted by α-Al_2O_3 (calcined for 4 h at 1473 K) in a ratio of 1:10. Spectra were measured in reflectance mode and converted into the Kubelka–Munk function $F(R)$ which is proportional to the absorption coefficient for sufficiently low $F(R)$ values. For a proper comparison of small variations of the shape of different experimental spectra, the $F(R)$ values of the latter were normalized, i.e., multiplied by a certain constant factor so as to obtain $F(R) = 1$ for the maximum of the spectrum. For in situ experiments, a heatable reaction chamber (Harrick) equipped with a temperature programmer (Eurotherm) and a gas-dosing system containing mass-flow controllers (Bronkhorst) was used. Deconvolution of the UV/VIS spectra into subbands was performed by the computer program GRAMS/32 (Galactic).

EPR spectra in the X-band ($\nu \approx 9.5$ GHz) were recorded with the cw spectrometer ELEXSYS 500-10/12 (Bruker) using a microwave power of 6.3 mW, a modulation frequency of 100 kHz, and a modulation amplitude of 0.5 mT. The magnetic field was measured with respect to the standard 2,2-diphenyl-1-picrylhydrazyl hydrate (DPPH). For temperature-dependent measurements in the range from 90 to 293 K, a commercial variable temperature control unit (Bruker) and a conventional EPR sample tube was used, while in situ EPR measurements during calcination in the range $293 < T/K < 773$ were performed in a homemade EPR flow reactor [29].

The selective reduction of NO with isobutane or ammonia was studied in a catalytic microflow reactor with a product analysis scheme that combined calibrated mass spectrometry, gas chromatography, and nondispersive IR photometry (NH_3). Feed gases containing 1000 ppm NO, 1000 ppm reductant (isobutane or ammonia), 2% O_2 in He were charged onto the catalyst at 30,000 h^{-1} for isobutane-SCR and 750,000 h^{-1} for NH_3-SCR. Generally, the catalytic runs were started with a thermal activation and stabilization treatment of the catalysts in flowing He at 550 °C (isobutane) or at 600 °C (NH_3). The activities were measured from the higher to the lower reaction temperatures. Under our experimental conditions, the only reaction product of NO observed in the limits of experimental accuracy was nitrogen; i.e., the NO conversions given are equal to N_2 yields.

3. Results and discussion

3.1. Catalytic activity

In Fig. 1, NO conversions achieved with the various Fe-ZSM-5 preparations and of the parent H-ZSM-5(A) are com-

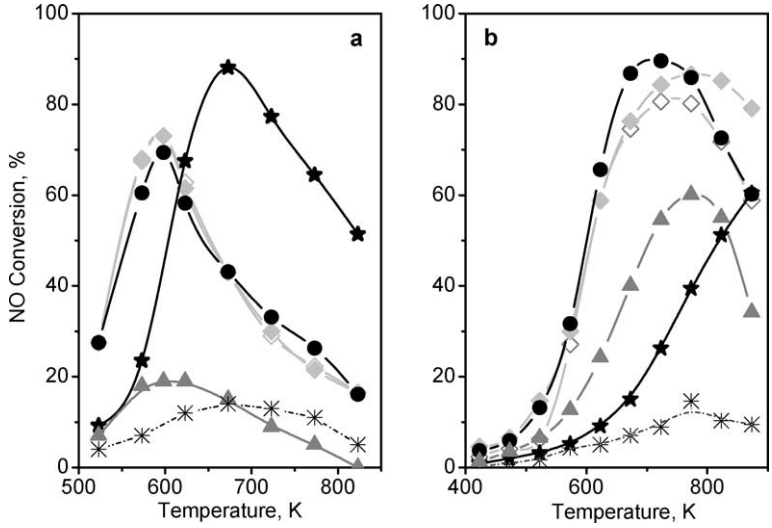

Fig. 1. NO conversions in the selective catalytic reduction of NO with isobutane (a) or NH_3 (b) over different Fe-ZSM-5 catalysts. Feed composition: 1000 ppm NO, 1000 ppm isobutane (or NH_3), 2% O_2 in He, at 30,000 h^{-1} (a) or 750,000 h^{-1} (b). ●, A(SSIE, W1, C5); ◇, A(CVD, W10, C0.5); ◆, A(CVD, W1, C5); ★ A(MR, C5); ▲, B(CVD, W1, C5); ∗, H-ZSM-5(A).

pared. Some of the data from isobutane-SCR have been already shown in [10]. A(MR, C5) is a new preparation the activity of which even exceeds that of the material described in [20]. As known from the literature, the activity of the catalysts with the ammonia reductant was found to be much larger than with isobutane [4,12,13].

Three different types of behavior can be identified for each reductant, but the details differ considerably. Catalysts prepared via gas-phase transport of $FeCl_3$ into H-ZSM-5(A) (A(SSIE, W1, C5), A(CVD, W1, C5), and A(CVD, W10, C0.5)) exhibit rather similar catalytic properties. In isobutane-SCR (Fig. 1a), the members of this reference group are hard to distinguish while in NH_3-SCR (Fig. 1b), the highest activity is obtained with A(SSIE, W1, C5). It should be noted that pore plugging, which is obvious with all catalysts from the pore volume data (see Experimental) is most severe with A(SSIE, W1, C5); hence, significant parts of the iron present may be included and not able to participate in catalysis. At high temperatures, the catalysts of the reference group exhibit remarkable differences in NH_3-SCR.

The remaining catalysts show a contrary behavior relative to this group. The material obtained by CVD of $FeCl_3$ into the defective ZSM-5 matrix B has lower activities with both reductants, but while its activity is very poor with isobutane it is still comparable with the other catalysts with ammonia where it achieves approximately half the conversions with half the Fe content. On the other hand, very high NO conversions are achieved with A(MR, C5), although at higher temperatures—at low temperatures, this catalyst falls short of the reference group as well. With ammonia, A(MR, C5) never achieves higher NO conversions than the remaining catalysts in accordance with the rule that a lower Fe content causes lower conversions. It should be noted, however, that the Fe content of A(MR, C5) is only 20% of that in B(CVD, W1, C5) and 10% of that in the reference-group catalysts. Therefore, a comparison on the basis of normalized reaction rates r_{NO}/Fe (reaction rate related to the total Fe content) is interesting. Table 1 reports such data for temperatures around 600 K (i.e., the temperature of peak NO conversion over the reference-group catalysts in isobutane-SCR). Although these data must be treated with some caution because they have been derived from measurements under integral conditions, they show that the intrinsic activity of the Fe sites is the highest also under these conditions. This is, in particular, true for isobutane-SCR while the advantage is less pronounced for NH_3-SCR.

Table 1
Normalized reaction rates, r_{NO}/Fe, for the SCR of NO with isobutane or NH_3 over Fe-ZSM-5 of different preparations

Preparation	Isobutane-SCR[a] $10^4 r_{NO}$/Fe, s^{-1} at 598 K	NH_3-SCR[a] $10^4 r_{NO}$/Fe, s^{-1} at 573 K
A(CVD, W1, C5)	4.1	42.2
A(CVD, W10, C0.5)	4.5	41.4
A(SSIE, W1, C5)	3.7	42.6
B(CVD, W1, C5)	2.2	36.7
A(MR, C5)	25.6[b]	79.1

[a] For conditions see legend to Fig. 1.
[b] From interpolated NO conversion.

3.2. Structural characterization

3.2.1. Assignment of EPR signals

EPR spectra of representative samples (A(SSIE, W1), A(CVD, W1, C0.5), and A(MR)), which were recorded at different temperatures, are displayed in Fig. 2. The spectra of all samples show three signals at effective g values of $g' \approx 6$, $g' \approx 4.3$ and $g' \approx 2$. Such signals were frequently detected in Fe-ZSM-5 [22,23,30,31] but also with Fe^{3+} ions

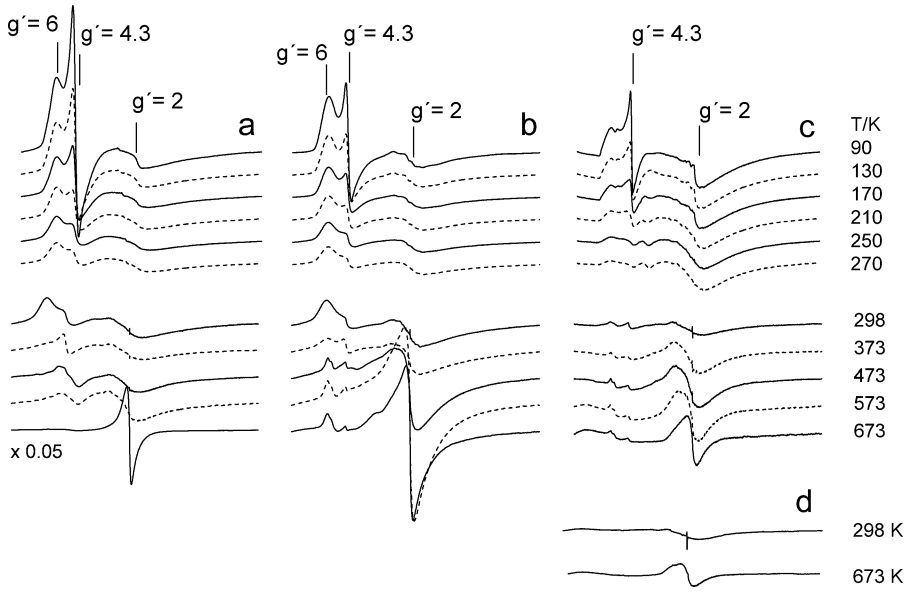

Fig. 2. EPR spectra of hydrated samples (a) A(SSIE, W1), (b) A(CVD, W1, C0.5), (c) A(MR)—uncalcined and (d) parent H-ZSM-5(A) during heating in air flow. Spectra of A(MR) and parent H-ZSM-5(A) are multiplied by a factor of 2.

in other oxide matrices. However, their assignment is by no means straightforward. The number and position of EPR transitions for Fe^{3+} ions observable in a powder spectrum depends sensitively on the local crystal field symmetry of these sites (reflected by the magnitude of the zero field splitting parameters D and E) and possible magnetic interactions between them. Signals at $g' \approx 4.3$ and $g' \geqslant 6$ arise from the $|-1/2> \leftrightarrow > 1/2|$ transition of isolated Fe^{3+} sites in strong rhombic ($D \gg h\nu$, $E/D = 1/3$, $g' \approx 4.3$) or axial distortion ($D \gg h\nu$, $E = 0$, $g' \approx 6$) when the zero field splitting is large in comparison to the microwave energy $h\nu$ [23,24,32]. This implies that an Fe^{3+} species giving rise to a line at $g' \approx 4.3$ is more strongly distorted than an Fe^{3+} site represented by a signal at $g' \approx 6$ due to the difference in the magnitude of E.

In zeolites, the line at $g' \approx 4.3$ is frequently assigned to Fe^{3+} sites incorporated in tetrahedral framework positions while a line at $g' \approx 6$ is assigned to isolated Fe^{3+} species in higher coordination numbers [23,30,31]. However, it must be stressed, that just from the signal position alone it is not possible to conclude whether the respective Fe ions are octathedrally or tetrahedrally coordinated since the signal position is governed by the magnitude of D and E, i.e., the extent of distortion of the Fe coordination. This distortion can arise from both tetrahedral and octahedral coordination. To draw conclusions on the number of ligands associated with the $g' \approx 4.3$ and 6 signals, additional aspects must be considered which are discussed in the following sections.

Given the preparation techniques, Fe-ZSM-5 samples studied in this work are not expected to contain Fe^{3+} in framework positions. However, XAFS measurements performed with hydrated Fe-ZSM-5 A(CVD, W1, C0.5) and A(MR, C5) samples in ambient atmosphere suggested that the latter do contain a certain amount of isolated, tetrahedrally coordinated Fe^{3+} ions [10,20]. Moreover, as will be shown below, an increase of the $g' \approx 4.3$ signal at the expense of $g' \approx 6$ and $g' \approx 2$ lines can be induced by dehydration, implying that the loss of water ligands leads to a lower coordination number. Therefore, we assign the EPR signal at $g' \approx 4.3$ to tetrahedrally coordinated Fe^{3+} species and the line at $g' \approx 6$ to isolated (presumably higher coordinated) Fe^{3+} species in less distorted extraframework positions.

Signals at $g' \approx 2$ can arise either from isolated Fe^{3+} in high symmetry (D, $E \approx 0$) or from Fe_xO_y clusters in which magnetic interactions between the Fe^{3+} ions average out the zero field splitting. For isolated, highly symmetric Fe^{3+} species, the signal intensity should follow the Curie–Weiss law, i.e., $I \sim 1/T$. It appears that both types of signal can be observed in the spectra: A narrow signal found at $g' \approx 2$ in A(MR) below 250 K (Fig. 2c) disappears upon heating while the broad superimposed signal, which is also present in the spectra of the other samples, narrows and increases with rising temperature. This points to antiferromagnetic interactions that collapse upon heating and suggests that the broad line at $g' \approx 2$ arises rather from neighboring than from isolated Fe^{3+} sites. Most probably such species are constituents of small oligonuclear Fe_xO_y clusters. It is rather unlikely, that a dimer Fe–O–Fe species can give rise to a $g' \approx 2$ signal with the observed temperature dependence. The existence of those moieties is discussed by several authors [14–17] in comparison to a similar species in the enzyme methane monooxygenase (MMO). However, it has to be noted, that in oxidized MMO those Fe^{3+}–O–Fe^{3+} dimers are EPR silent due to spin pairing ($S = 0$). In the partially reduced MMO a signal with g' values of 1.94, 1.86, and 1.75 was observed at 8 K for an oxo-bridged binuclear iron cluster and in the completely reduced MMO a single line at $g' \approx 16$ has been recorded at 8 K which was assigned to a dimer composed of two ferromagnetically coupled high-spin Fe^{2+} centers [33]. None of those signals is observed in the Fe-ZSM-5 samples studied in this work. Therefore, we think that the presence of an oxo-bridged Fe dimer similar to that in MMO is highly questionable in our Fe-ZSM-5, although it cannot be rigorously excluded. Theoretically, a Fe^{3+}–O–Fe^{3+} dimer species could contribute to the $g' \approx 2$ signal when its Neel temperature is exceeded.

3.2.2. Assignment of UV/VIS signals

The UV/VIS spectra of Fe-ZSM-5 zeolites presented in this work have been deconvoluted into subbands to facilitate assignment to different Fe species. In principle, two ligand-to-metal charge-transfer (CT) transitions, $t_1 \rightarrow t_2$ and $t_1 \rightarrow e$, are to be expected for a Fe^{3+} ion [34]. For isolated Fe^{3+} sites they give rise to bands below 300 nm, whereby their particular position depends on the number of ligands. Thus, CT bands of isomorphously incorporated tetrahedrally coordinated Fe^{3+} ions have been observed at 215 and 241 nm in Fe–silicalite [27] while a band at 278 nm is detected for isolated octahedral Fe^{3+} sites in Al_2O_3 [35]. Although a clear discrimination of CT bands of isolated Fe^{3+} sites in tetrahedral and higher coordination is not straightforward due to their similar wavelength range, these values suggest that CT bands of Fe^{3+} are red-shifted with increasing number of coordinating oxygen ligands. The same trend has been observed accordingly also for V^{5+} species [36].

In the UV/VIS spectrum of sample A(MR) two intense bands appear at 228 and 290 nm (Fig. 3b). Previous EXAFS measurements revealed that this sample is dominated by isolated Fe^{3+} sites with a mean coordination number between 4 and 6, suggesting that these Fe species are in both tetrahedral and higher coordination [20]. In agreement with these results we assign the two strong bands in Fig. 3b to isolated Fe^{3+} sites in tetrahedral (228 nm) and higher coordination (290 nm). For spectra deconvolution, only one CT band has been used for each of the two isolated Fe^{3+} species, since separate bands for the two possible CT transitions of each type of Fe^{3+} species ($t_1 \rightarrow t_2$ and $t_1 \rightarrow e$) are not resolved in the experimental spectrum.

According to the literature, CT bands between 300 and 400 nm are assigned to octahedral Fe^{3+} in small oligomeric Fe_xO_y clusters [27] while bands above 450 nm arise from larger Fe_2O_3 particles as can be seen, too, from the spec-

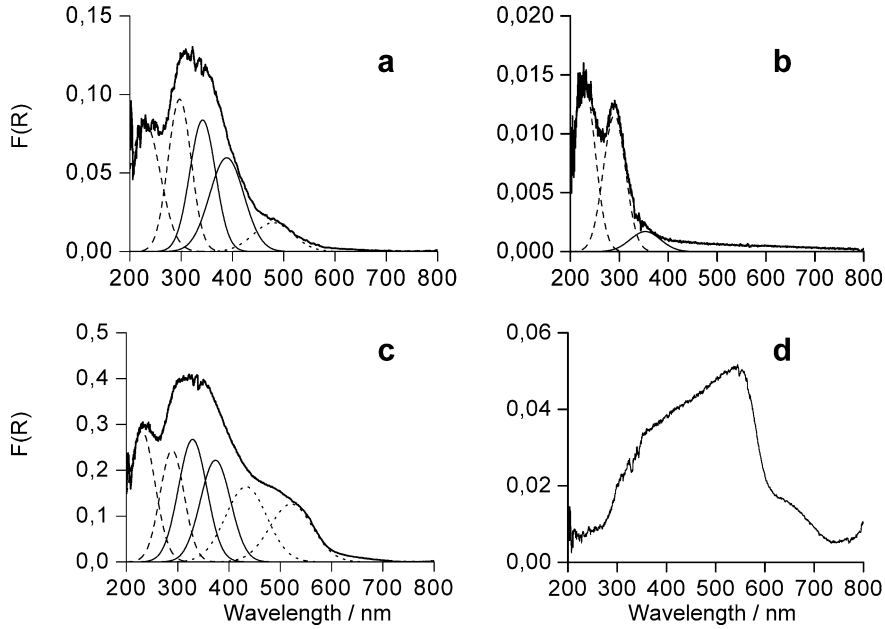

Fig. 3. UV/VIS diffuse reflectance spectra of hydrated as-prepared samples, compared with α-Fe_2O_3; experimental spectra, thick solid lines; deconvoluted subbands, thin lines; assignments: - - - isolated Fe^{3+}, — small oligomeric Fe_xO_y moieties, ⋯ extended Fe_2O_3-like clusters, (a) A(CVD, W1), (b) A(MR), (c) A(SSIE, W1), (d) α-Fe_2O_3.

trum of the reference sample α-Fe_2O_3 (Fig. 3d). In general, a $t_1 \rightarrow t_2$ and a $t_1 \rightarrow e$ transition should be expected, too, for Fe^{3+} in cluster-like Fe_xO_y species. However, light absorption in the spectra of Figs. 3a and c above 300 nm occurs in a very broad range, suggesting the superposition of those bands for a variety of slightly different small oligonuclear Fe_xO_y clusters and larger Fe_2O_3 species. Thus, for spectra deconvolution the lowest possible number of subbands in the range above 300 nm has been used that was needed to obtain a satisfactory fit of the experimental spectrum. This procedure is regarded to be acceptable, although a deconvolution of a broad and poorly structured experimental spectrum into subbands by mathematical means is always arbitrary to a certain extent. The subbands above 300 nm must be understood in terms of reflecting a certain distribution of slightly different cluster geometries rather than representing a certain number of different individual cluster species. The percentage of the subbands with respect to the total area of the experimental spectrum has been multiplied with the overall Fe content (accurately determined by both EXAFS and ICP-OES) to obtain a rough estimate of the percentage of the different Fe species in the samples (Table 2). Being aware that the obtained values in Table 2 are inaccurate to a certain degree due to the deconvolution procedure, they are nevertheless regarded to be helpful for a comparison of different samples.

Table 2
Percentage of the area of the subbands (I_1 at $\lambda < 300$ nm, I_2 at $300 < \lambda < 400$ nm, and I_3 at $\lambda > 400$ nm) derived by deconvolution of the UV/VIS-DRS spectra (see Figs. 3, 4, 6, and 7) and corresponding Fe percentage derived from total Fe content determined by XAFS [10,20]

Catalyst	I_1[a] (%)	Fe_1 (wt%)	I_2[b] (%)	Fe_2 (wt%)	I_3[c] (%)	Fe_3 (wt%)
A(MR)	91	0.45	9	0.05	–	–
A(MR, C5)[d]	83	0.41	17	0.09	–	–
A(CVD,W1)	47	2.53	45	2.43	8	0.43
A(CVD,W1,C0.5)	27	1.46	36	1.94	37	2.00
A(CVD,W1,C0.5) used	25	1.35	31	1.67	44	2.37
A(CVD,W1,C5)	27	1.46	35	1.89	38	2.05
A(CVD,W1,C5) used	22	1.19	30	1.62	48	2.59
A(CVD,W10)	46	2.30	47	2.35	7	0.35
A(CVD,W10, C0.5)[e] used	27	1.35	36	1.80	36	1.80
A(SSIE, W1)	32	1.66	37	1.90	31	1.62
A(SSIE, W1, C5)	30	1.56	32	1.66	38	1.98
B(CVD,W1)	28	0.73	45	1.17	27	0.70
B(CVD,W1,C5)	26	0.68	38	1.0	35	0.91

[a] Isolated Fe^{3+} in tetrahedral and higher coordination.
[b] Small oligomeric Fe_xO_y clusters.
[c] Large Fe_2O_3 particles.
[d] Calcined at 823 K, spectrum not shown.
[e] Spectrum in Fig. 6b.

3.3. Influence of the mode of Fe incorporation

With the exception of the narrow signal at $g' \approx 2$, the shape and behavior of the EPR signals in the low-temperature range (90–270 K) are rather similar for the three samples, but the absolute intensities decrease in the order A(SSIE, W1) > A(CVD, W1, C0.5) > A(MR). The signals at $g' \approx 6$ and $g' \approx 4.3$, and also the narrow one at $g' \approx 2$ in A(MR), decrease with rising temperature as expected for paramagnetic behavior, whereby the intensity loss of the $g' \approx 4.3$ signal is stronger, suggesting shorter relaxation times in comparison to the Fe^{3+} species reflected by $g' \approx 6$. At $T \geqslant 373$ K those signals become narrower and better resolved. This is attributed to the loss of water mole-

cules from the pores which are assumed to be located in the coordination sphere of the Fe^{3+} ions and give rise to a certain distribution of the zero field splitting parameters which enhances the linewidth.

The broad signal at $g' \approx 2$ does not show Curie-like behavior. In the high-temperature range it increases and narrows suddenly. This suggests that the samples contain antiferromagnetically coupled Fe_xO_y species with a Neel temperature of $T_N > 573$ K for sample A(SSIE, W1) and $T_N > 373$ K for samples A(CVD, W1, C0.5) and A(MR). Above T_N those species become paramagnetic and contribute to the EPR signal. A strong line narrowing seen in particular in A(SSIE, W1) is due to spin–spin exchange interaction which is most effective for well-ordered, large clusters. Those species were earlier detected in sample A(SSIE) (i.e., without washing) by XRD, TPR, and XAFS [10]. It is not unexpected that they remain also in the washed material. Intensity increase and exchange narrowing are much less pronounced in sample A(CVD,W1, C0.5); hence, the clusters have a smaller size and a lower degree of order. In the latter sample, the signal at $g' \approx 2$ is anisotropic. This suggests that the signal is not due to a particular species with defined geometry but to a superposition of Fe_xO_y species with a certain size distribution. The results described confirm assumptions suggested in [10] to explain the striking contradictions between EXAFS and Mössbauer results on Fe-ZSM-5 prepared via the CVD route: disordered clusters cannot be detected by methods that rely on wave interference as XRD and EXAFS, but are seen by methods based on magnetic interactions. The reason for the lack of order in these clusters (as opposed to the extrazeolite aggregates in A(SSIE, W1) is most likely an intrazeolite location; i.e., the zeolite structure may have been partly destroyed and included during particle growth. This has been suggested in [10] on the basis of XPS data and has been visualized in [17] by scanning transmission electron micrographs.

Note that the temperature dependence of the broad $g' \approx 2$ signal in sample A(MR) indicates clearly the presence of Fe_xO_y clusters (Fig. 2c), although the lower intensity and the larger linewidth suggest that they are much less abundant and smaller than in samples A(SSIE, W1) and A(CVD, W1, C0.5). As noted above, these species were not detected by XAFS [20], illustrating the power of EPR spectroscopy for such investigations. Even the parent H-ZSM-5 which contains only 0.05% Fe shows a small $g' \approx 2$ line with non-Curie behavior, indicating that it is not free of small Fe_xO_y clusters. Moreover, signals at $g' \approx 4.3$ and 6 were not detected in the parent H-ZSM-5. This shows clearly that the respective Fe^{3+} species are introduced by the various Fe loading procedures.

Experimental UV/VIS spectra of the samples in the as-prepared state (i.e., CVD and MR before calcination, while SSIE is calcined during the preparation) are presented together with deconvoluted subbands in Fig. 3. The relative percentage of the area of these subbands with respect to the total spectral intensity is summarized in Table 2. From Fig. 3 and Table 2 it is evident that sample A(MR) is dominated by isolated Fe^{3+} sites with a certain amount of small oligomeric Fe_xO_y moieties (band at 353 nm) also present. Those clusters are dominating species in samples A(CVD, W1) and A(SSIE, W1) while the latter contains also a considerable amount of large Fe_2O_3 particles.

By taking into account both the EPR and UV/VIS results, it can be concluded that each of the three Fe-ZSM-5 samples contains at least two different Fe^{3+} single sites, probably in tetrahedral and higher coordination as reflected by EPR signals at $g' \approx 4.3$ and $g' \approx 6$ and by UV/VIS CT bands below 300 nm. A third kind of isolated Fe^{3+} ions in less distorted environment is present in A(MR), but it cannot be excluded that it is present in the other samples as well, but is masked by the EPR cluster signal at $g' \approx 2$. Besides the different isolated Fe^{3+} sites, Fe_xO_y aggregates are formed, the amount and size of which increases considerably in the order A(MR) $\ll$ A(CVD, W1) $<$ A(SSIE, W1). The data reveal that the mechanochemical route is most effective in introducing preferably isolated Fe^{3+} sites into pore positions of H-ZSM-5.

It should be noted that none of the characterization techniques applied previously [10,20] was able to distinguish coexisting different isolated Fe^{3+} species. Furthermore, XAFS data of sample MR do not reflect any Fe_xO_y clusters, although they are clearly detected by EPR and UV/VIS-DRS. This illustrates the benefit of the two techniques for the characterization of complex solid materials like Fe-ZSM-5.

3.4. Influence of heat treatment

The as-prepared states discussed above are not really comparable because A(SSIE, W1) had been subjected to a higher temperature than A(CVD, W1) during preparation. Heat treatment; e.g., the calcination in air at 873 K, usually performed before catalytic experiments [10,20] causes indeed significant structural changes as demonstrated in Fig. 4. In this figure, EPR and UV/VIS spectra of sample A(CVD, W1) are shown before calcination as well as after calcination in air at 873 K using heating rates of 5 and 0.5 K/min. It is clearly seen from the EPR spectra (Fig. 4a) that signals of isolated Fe^{3+} sites at $g' \approx 6$ and $g' \approx 4.3$ lose intensity upon calcination while the signal at $g' \approx 2$ increases. This suggests that initially isolated Fe sites aggregate to form Fe_xO_y clusters. This effect seems to be slightly favored by higher heating rates. In the corresponding UV/VIS spectra (Fig. 4b), light absorption above 400 nm being characteristic of extended Fe_2O_3-like clusters is somewhat higher after calcination with 5 K/min than with 0.5 K/min (Fig. 4, Table 2). Clustering of isolated Fe species upon calcination in air has been observed for all FeZSM-5 samples including A(SSIE, W1) (Table 2). It appears that Fe_xO_y cluster formation is favored by moisture remaining in the zeolites after washing.

EPR, on the other hand, reveals additional features of the calcination process as shown in Fig. 5. In Figs. 5a and

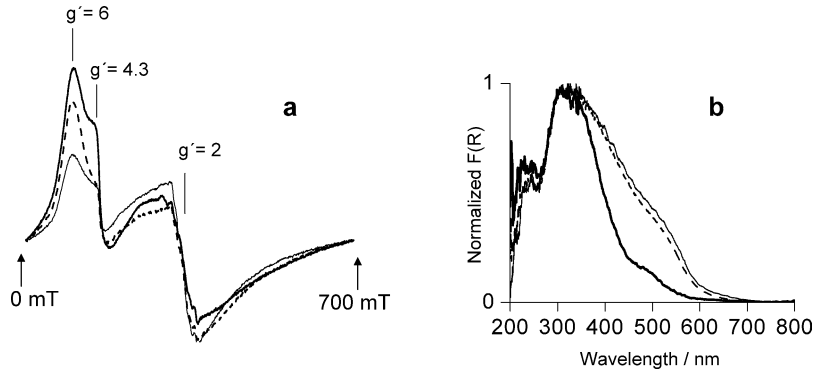

Fig. 4. Structural changes of the iron phase in sample A(CVD, W1) during calcination as seen by EPR (a) and UV/VIS spectroscopy (b); spectra recorded from hydrated samples at room temperature; before calcination (thick solid line), after calcination at 873 K with a heating rate of 0.5 K/min (dashed line), and after calcination at 873 K with a heating rate of 5 K/min (thin solid line).

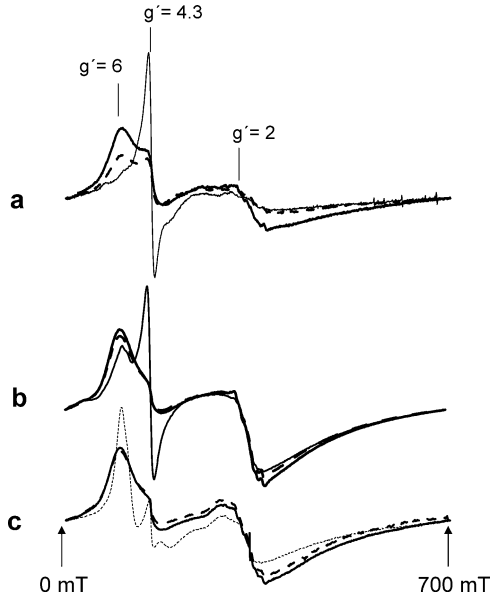

Fig. 5. Structural changes of the isolated Fe species in sample A(CVD, W1) during calcination; EPR spectra recorded at room temperature; initial hydrated state (thick solid line), after 2 h evacuation at 293 K (thin solid line), after 2 h calcination in air at 773 K (dotted line), and after reexposing to the ambient atmosphere (dashed line); initial states: (a) as-prepared sample A(CVD, W1); (b and c) calcined sample A(CVD, W1, C0.5) after long-term storage at the ambient atmosphere.

b, the effect of a room-temperature evacuation and subsequent contact with the ambient atmosphere is compared for the uncalcined and the calcined samples A(CVD, W1) and A(CVD, W1, C0.5), where the latter had been rehydrated in ambient atmosphere between calcination and EPR experiment for an extended period of time. Fig. 5c shows the effect of a thermal treatment in air at 773 K (instead of room-temperature evacuation) on the calcined and rehydrated sample A(CVD, W1, C0.5). It can be seen that evacuation of the uncalcined A(CVD, W1) material leads to a complete disappearance of the signal at $g' \approx 6$ while the one at $g' \approx 4.3$ increases strongly and becomes narrower (Fig. 5a). This shift is largely reversed by contact with ambient atmosphere. For the calcined but rehydrated sample A(CVD, W1, C0.5) the $g' \approx 6$ signal remains upon room-temperature evacuation but has lost much intensity to that at $g' \approx 4.3$ (Fig. 5b). When, instead of 2 h evacuation at room temperature, the latter sample is again thermally treated in air at 773 K, very different changes are induced (Fig. 5c): Now there is just a narrowing of the signals at $g' \approx 6$ and $g' \approx 4.3$ and the effect is completely reversible upon exposure to the ambient atmosphere.

An explanation of this behavior may set out from the assumption that $[FeCl_2]^+$ cations deposited on cation sites during the CVD step [6,15] [Eq. (1)] are hydrolyzed during the washing step. In this process, part of the iron species may acquire a distorted coordination sphere with a coordination number of 6 or 5 made up of water, charge-balancing OH groups, and, possibly, oxygen of the zeolite wall, which is reflected in the signal at $g' \approx 6$ [e.g., Eq. (2)]

$$H^+ + FeCl_3 \rightarrow [FeCl_2]^+ + HCl, \quad (1)$$

$$[FeCl_2]^+ + nH_2O + mO_z \rightarrow \left[Fe(H_2O)_n(O_z)_m(OH)_2\right]^+ + 2HCl \quad (2)$$

$(m + n = 3 \text{ or } 4)$.

Upon room-temperature evacuation, the water ligands may be reversibly removed, and the respective Fe species contribute to the signal at $g' \approx 4.3$ which might arise from tetrahedral Fe species as frequently discussed in the literature (Fig. 5a). After calcination, however, if contact with the humid air is avoided, the coordination of most Fe ions is much different (Fig. 5c, dotted line). The difference is obviously caused by the more severe effect of the thermal treatment as opposed to room-temperature evacuation and consists presumably in a condensation of OH groups, e.g., the charge-balancing OH groups on the Fe^{3+} ion. This process would lead to a cation with an extraframework oxygen coordinated to 4 or 5 framework oxygens (Eq. (3), with a higher probability for $p = 4$ due to the sterical conditions in the zeolite). We believe that this species gives rise to the narrow signal at $g' \approx 6$ after calcination (Fig. 5c), which is a typical feature of this type of mononuclear Fe sites in the dehydrated state.

There is, however, also a minority species in tetrahedral coordination ($g' \approx 4.3$).

$$\left[\mathrm{Fe}(\mathrm{H_2O})_n(\mathrm{O}_z)_m(\mathrm{OH})_2\right]^+ \rightarrow \left[(\mathrm{O}_z)_p\mathrm{FeO}\right]^+ \quad (p = 4 \text{ or } 5 \text{ for } g' \approx 6, \text{ and } p = 3 \text{ for } g' \approx 4.3). \qquad (3)$$

Upon contact with the humid ambient atmosphere, the outer coordination sphere of the Fe species is influenced by adsorbed water, which results in slightly different distortions at different lattice positions and causes the broadening of the signals, in particular that at $g' \approx 6$, which can be seen in Fig. 5c. The reversal of the structural change upon dehydration (probably rehydration of the Fe=O units), however, appears to proceed much more slowly: This is suggested by a comparison of the spectra after 2 h evacuation in Figs. 5a and b. In contrast to the initial sample in Fig. 5a, the one in Fig. 5b had been calcined but stored in ambient atmosphere for an extended period of time. The narrow $g' \approx 6$ signal typical of the dehydrated structures is still left to an appreciable extent in the latter sample after 2 h evacuation (Fig. 5b); i.e., prolonged storage in the ambient atmosphere led to only incomplete rehydration of the dehydrated Fe site. Unfortunately, it is difficult to predict on the basis of this information which structure of the Fe cation will be present under reaction conditions: while the higher temperatures should favor dehydration, there is water present in the atmosphere in significant amounts strongly depending on the water content of the feed. This question will be subject to further in situ EPR studies.

3.5. Influence of washing intensity

It has been reported in the literature that thorough washing is crucial for the formation of highly dispersed Fe structures [10,15,37]. In our study, the influence of the washing step was checked by performing the washing procedure of A(CVD) with a total amount of 1 L or 10 L water per 5 g catalyst (A(CVD, W1) and A(CVD, W10), respectively.) The UV/VIS spectra of these samples are compared in Fig 6a. After washing with 10 L water, the light absorption above 400 nm is weaker in comparison to after the short washing procedure, which indicates that intense washing diminishes the amount of big Fe_xO_y clusters slightly (Table 1). This has been concluded earlier from TPR and Mössbauer measurements, although these had been performed with the respective A(CVD, W1) and A(CVD, W10) samples after calcination and use in the SCR reaction [10]. For comparison, the UV/VIS spectra of these (used) samples are given in Fig. 6b. As shown above, thermal stress (calcination or use in the SCR reaction, which is initiated by a thermal activation/stabilization process) favors aggregation of isolated Fe sites markedly. Even after use in catalysis, however, the better dispersion of the iron species in the intensely washed material can be traced by a decreased absorption above 400 nm (solid line). This is also confirmed by temperature-dependent EPR measurements (Figs. 6c and d). In the spectra of A(CVD, W1, C0.5) after catalysis, an intense narrow signal appears at $g' \approx 2$ above 373 K, indicating the presence of extended Fe_xO_y clusters with marked antiferromagnetic coupling (Fig. 6c). In contrast, the increase of this line in A(CVD, W10, C0.5) after catalysis is much less pronounced, which suggests a weaker antiferromagnetic coupling due to a smaller cluster size (Fig. 6d).

3.6. Influence of the SCR reaction

In Fig. 7, EPR and UV/VIS spectra of catalyst A(CVD, W1, C0.5) before and after use in the SCR of NO with isobutane (duration 1 working day) are compared in order to trace structural changes that might occur in a precalcined catalyst under reaction conditions. In the EPR spectrum (Fig. 7a), the signal at $g' \approx 6$ has almost disappeared while the signal at $g' \approx 4.3$ is virtually not effected. At the same time, the cluster signal at $g' \approx 2$, has grown enormously. In the corresponding UV/VIS spectrum (Fig. 7b), light absorption above 400 nm reflecting extended Fe_2O_3-like clusters is only slightly more pronounced after catalysis: The contribution of the subbands above 400 nm to the total intensity increases from 37 to 44% after the catalytic run (Table 2). This is almost exclusively at the expense of subbands between 300 and 400 nm while the contribution of the isolated sites remains constant. Hence, during catalysis, large oxide particles are formed rather from small oligomeric moieties than from isolated Fe sites.

This conclusion is also supported by the apparent contradiction between the extent of particle growth indicated by the EPR and the UV/VIS spectra (Figs. 7a and b). While the increase of the EPR cluster signal at $g' \approx 2$ by exposure to the catalytic conditions is huge, the relative intensity of the corresponding UV/VIS subbands above 300 nm changes only slightly after reaction. Obviously, the strong increase of the EPR signal at $g' \approx 2$ after reaction is mainly due to intensified spin–spin exchange interactions between neighboring Fe sites which is probably caused by lattice ordering in larger Fe_xO_y clusters.

The strong attenuation of the $g' \approx 6$ line suggests that Fe species reflected by this signal, are modified in the catalytic reaction while those related to the $g' \approx 4.3$ line remain unchanged. The UV/VIS data (Table 2), on the other hand, imply that this modification is not caused by cluster formation or reduction but just by a change in the Fe coordination geometry. In our recent in situ EPR studies of the direct N_2O decomposition and the SCR of N_2O by CO over different Fe-MFI catalysts we have observed that the $g' \approx 6$ EPR signal changes upon contact with feed components while the line at $g' \approx 4.3$ remains virtually unchanged [38]. Similar effects were found during in situ EPR investigations of samples A(MR) and A(CVD, W1, C0.5) during the SCR of NO by *i*-butane [39]. Other authors also observed that the $g' \approx 6$ signal in Fe-ZSM5 vanishes after use of the material as a catalyst for different reactions, which was attributed to the high activity of these particular Fe^{3+} sites [2,40,41]. Kubánek et al. derived a linear correlation between the $g' \approx 6$ signal in-

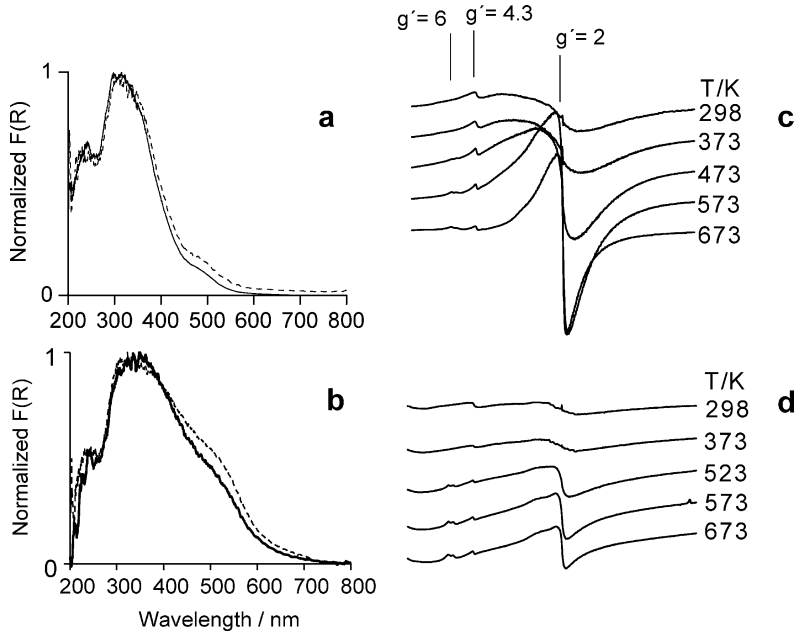

Fig. 6. Influence of the washing intensity on the Fe dispersion in Fe-ZSM-5. UV/VIS spectra of (a) as-prepared hydrated samples A(CVD, W1) (dashed line) and A(CVD, W10) (solid line) and (b) calcined hydrated samples A(CVD, W1, C0.5) (dashed line) and A(CVD, W10, C0.5) (solid line) after use in the SCR reaction; EPR spectra of the used hydrated samples A(CVD, W1, C0.5) (c) and A(CVD, W10, C0.5) (d). Samples were recalcined after catalysis in air at 823 K.

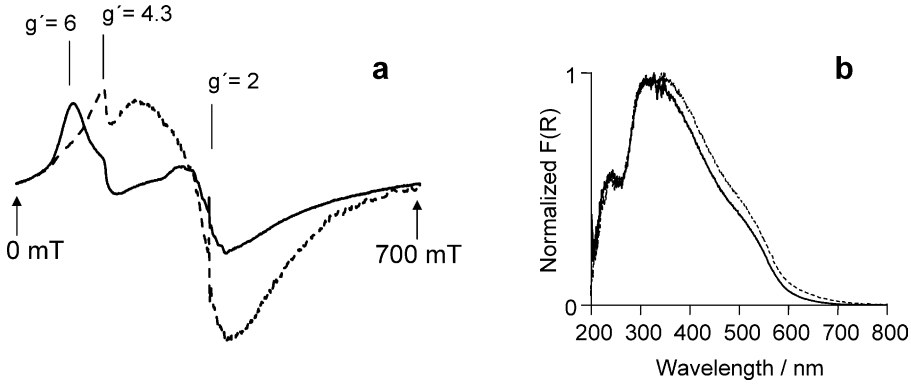

Fig. 7. Changes of the Fe species after use in the SCR with isobutane. EPR (a) and UV/VIS spectra (b) of hydrated sample A(CVD, W1, C0.5) measured at room temperature before (thick solid line) and after use in the SCR of NO (broken line). Samples were recalcined after catalysis in air at 823 K.

tensity and the activity of Fe-ZSM-5 in the conversion of benzene to phenol by N_2O while no change of intensity was observed for the $g' \approx 4.3$ signal [42]. It was concluded that Fe^{3+} species reflected by the latter signal are mainly located in extraframework Al–O clusters that had been formed by a steaming pretreatment and, therefore, do not participate in the catalytic reaction.

Fe-ZSM-5 catalysts used in the present work have not been pretreated by steaming. Moreover, no indication for a partial lattice damage upon use in the SCR reaction was found that could give rise to dealumination and inclusion of Fe in an extraframework Al–O phase. However, it is possible that the Fe species responsible for the unchanged $g' \approx 4.3$ signal may be unable to extend their coordination sphere by adsorbing reactant molecules. It seems not unlikely that those Fe^{3+} species could be located in the γ-sites of the MFI structure. It was found that the latter represent sites of strongest distortion [43]. This would agree pretty well with the fact that a signal at $g' \approx 4.3$ arises, too, from Fe^{3+} sites in the strongest possible distortion. Although Fe^{3+} species in γ sites should be accessible by reactant molecules from the main channel [43], their confinement within the rather narrow pocket-like g site could prevent the necessary coordination of reactant molecules from the gas phase.

As suggested by EPR and UV/VIS results discussed above (Fig. 7, Table 2), large oxide particles seem to be preferably formed from small oligomeric moieties during use in the SCR reaction while the amount of isolated Fe sites remains virtually unchanged. Interestingly, no deactivation occurs on the time scale of the experiments performed despite those significant structural changes. The fact that the amount of small oligonuclear clusters decreases in fa-

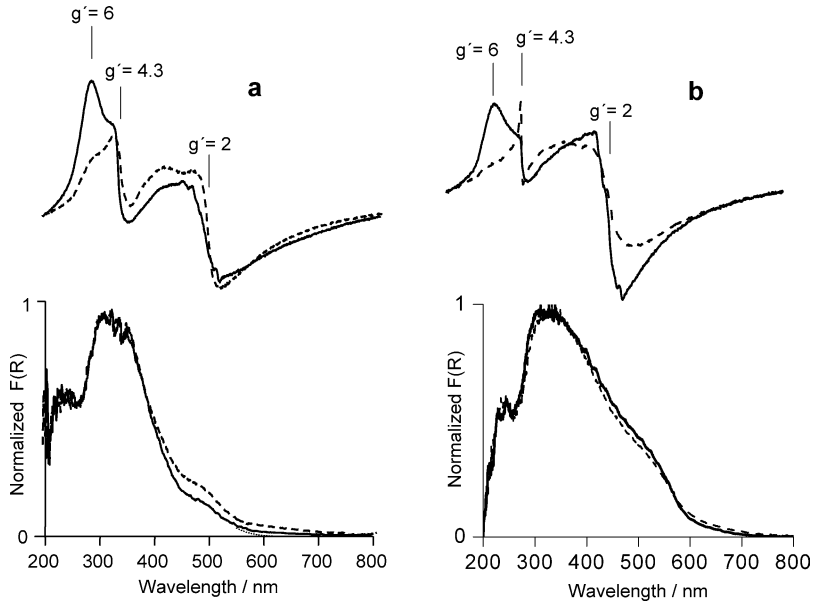

Fig. 8. Influence of the Si/Al ratio and the lattice perfection on the structure of Fe species in Fe-ZSM-5. EPR and UV/VIS spectra (measured from hydrated samples at room temperature) of materials prepared with zeolites ZSM-5(A) and ZSM-5(B), (a) as-prepared samples B(CVD, W1) (dashed line) and A(CVD, W1) (solid line); (b) calcined samples B(CVD, W1, C5) (dashed line) and A(CVD, W1, C5) (solid line).

vor of large oxide particles while isolated Fe sites persist during reaction may indicate that the latter are the active Fe sites of the SCR reaction. However, the changes between the amounts of oligomers and large aggregates (Table 2) are too small to safely exclude a contribution of the clustered phases. On the other hand, since EPR reflects a strong ordering tendency in the clustered phase and it is unlikely that the catalytic activity of clusters will be improved by increasing structural perfection, the structural changes observed on the whole support the view that isolated Fe sites play a deciding role in the SCR reaction as proposed, for instance, in [10,19,20].

3.7. Influence of the Al content and defect density of the parent ZSM-5 matrix

Fe-ZSM-5 was also prepared via CVD of $FeCl_3$ into the ZSM-5 matrix B, which has a lower Si/Al ratio than Matrix A (≈ 40 vs ≈ 14). This, in turn, leads to a lower number of H^+ sites available for exchange by Fe ions, and a large amount of internal silanol groups, most likely silanol nests [10]. As expected, the total Fe content in sample B(CVD, W1) is lower than in sample A(CVD, W1), but the Fe/Al ratio of 1.13 shows that sample B(CVD, W1) is even more overexchanged than the latter (Fe/Al ≈ 0.9). It is therefore in agreement with expectations that the EPR signals for isolated Fe sites at low magnetic field are less intense for the uncalcined sample B(CVD, W1) than for A(CVD, W1) while the cluster signal at $g' \approx 2$ is larger (Fig. 8a). A slightly higher percentage of extended Fe_2O_3-like clusters in sample B(CVD, W1) is also evident from UV/VIS data (Fig. 8a, Table 2).

Interestingly, this trend is not retained for the calcined samples (Fig. 8b). Calcination with a heating rate of 5 K/min leads to a slightly less pronounced formation of large Fe_2O_3-like aggregates in sample B(CVD, W1, C5) compared to A(CVD, W1, C5) as evident from both EPR and UV/VIS spectra. This may be explained by the presence of silanol nests in the sample, which may serve as additional nuclei for aggregation as has been suggested earlier on the basis of FTIR, Mössbauer, and EXAFS data [10]. In well-structured HZSM-5 matrices Fe_xO_y clusters being formed upon calcination have been shown to migrate toward the external crystal surface where they can grow further in size [17]. In contrast, silanol nests present in highly defective matrices could keep the clusters inside the crystal, thus preventing their further growth. Remarkably, the EPR signal at $g' \approx 6$ is extremely weak or completely absent in sample B(CVD, W1, C5); instead, the signal at $g' \approx 4.3$ is more pronounced.

3.8. Active sites for SCR catalysis

The characterization studies confirm the structural complexity of the iron species obtained by CVD of $FeCl_3$ into H-ZSM-5 and related methods and support the skepticism toward quantitative conclusions from EXAFS spectra of such materials, as has been expressed earlier in [10,11]. This complexity is a serious obstacle for the identification of the active sites for selective NO reduction. However, by comparing trends in the SCR activity data and the structural data obtained in this study, some suggestions can be derived even from the work with these highly nonideal materials.

An effort to find correlations between the concentration of Fe species as analyzed by UV/VIS (Table 2) and catalytic properties may embark from the very similar behavior

of some catalysts with both the isobutane and the ammonia reductant (reference group A(SSIE, W1, C5), A(CVD, W1, C5), and A(CVD, W10, C0.5)). The comparison of the species distribution in these materials (Table 2) shows that the amounts of all sites vary to a certain extent so that a correlation is not possible. This is not unexpected because the species distinguished by UV/VIS in fact represent several entities, e.g., at least 3 isolated sites, one of which ($g' \approx 4.3$ in EPR) appears to be unable to extend its coordination sphere by adsorbing molecules from the gas phase, oligomers of different nuclearity (starting with dimers), and particles of different size. The comparison with the activity data of A(MR, C5) shows, however, that the participation of isolated sites in the catalytic reactions is highly likely. This sample, which achieves the highest normalized reaction rates in both reactions (Table 1), and with isobutane even the highest NO conversions in a broad temperature range, does not contain particles and only a very small amount of oligomers while the quantity of isolated sites is somewhat lower than in the reference-group catalysts. While particles can be therefore safely rejected as active sites, the extremely low quantity of oligomers (more than an order of magnitude less than in the reference-group catalysts) strongly discourages an assignment of the catalytic activity exclusively to oligomers. The data imply rather that mononuclear Fe species participate in SCR catalysis, probably together with oligomeric entities. A similar suggestion has been made above for isobutane-SCR on the basis of the observation that significant ordering of the clustered species occurs during catalysis (Fig. 7) without concomitant changes in the catalytic behavior.

For NH_3-SCR, the participation of several types of sites is nicely illustrated by the behavior of the catalyst prepared with the silica-rich matrix H-ZSM-5(B) – B(CVD, W1, C5). While this material fails completely in isobutane-SCR, it is ranked between A(MR, C5) and the reference-group catalysts in NH_3-SCR (Fig. 1), where it exhibits almost the same normalized reaction rate as the reference-group catalysts (Table 1). The considerably higher activity as compared with A(MR, C5) (Fig. 1) is achieved with an only slightly larger smaller amount of isolated entities (0.68 vs 0.41 wt%, cf. Table 2); hence aggregated species will contribute to activity. On the other hand, the latter are hardly present in A(MR, C5); hence they cannot be the single type of active site for NH_3-SCR. It appears therefore that all iron accessible may be part of active sites for NH_3-SCR. In addition, it should be noted that B(CVD, W1, C5) has only a very low acidity as has been found in FTIR [10] and ammonia-TPD studies. This indicates that acidity is not of importance for NH_3-SCR with Fe-ZSM-5, at least in the presence of active sites of the clustered type. The reason for the failure of B(CVD, W1, C5) with isobutane cannot be conclusively explained. It may be due to the absence of a particular Fe site that is summarized but not distinguished by UV/VIS (e.g., a particular mononuclear site) or to the absence of sufficient acidity. The role of acidity in isobutane -SCR with Fe-ZSM-5 will be discussed elsewhere.

In NH_3-SCR, NO conversion drops at high temperatures for all catalysts except A(MR, C5). The decreased NO conversion is accompanied by an almost constant NH_3 conversion of ca. 90% (not shown); i.e. part of the reductant is oxidized at higher temperatures to N_2 [4,43]. With A(MR, C5), NH_3 conversion equals NO conversion within the limits of experimental accuracy up to 873 K (not shown). From this it may be concluded that the ammonia oxidation is catalyzed by the clustered species (oligomers, particles), although the details of the high-temperature behavior (differences between A(SSIE, W1, C5), A(CVD, W1, C5), A(CVD, W1, C0.5)) are not yet understood. A similar discussion is possible for isobutane-SCR: Here, the catalyst with a negligible amount of clustered entities achieves high NO conversions still at 700–800 K where those with large amounts of oligomers and particles are much less selective for NO reduction. The competition of nonselective oxidation starts at a lower temperature for the isobutane than for the ammonia reductant, which may reflect a different propensity of the reductants to become oxidized over Fe sites. From this, an improved catalyst for both SCR processes should contain increased amounts of mononuclear species with as low as possible quantities of clustered entities. Studies of catalysts prepared with this intention are currently under way.

4. Conclusions

Fe-ZSM-5 catalysts prepared by different techniques from H-ZSM-5 (solid-state ion exchange, chemical vapor deposition of $FeCl_3$ with variations of the subsequent washing and calcination steps, mechanochemical treatment with $FeCl_3$), which had been previously characterized by XRD, EXAFS, Mössbauer spectroscopy, TPR, FTIR, and XPS, have been additionally analyzed by EPR and UV/VIS diffuse reflectance spectroscopy (DRS)—ex situ after preparation, after calcination and after use in the selective catalytic reduction of NO as well as in situ during calcination. It has been found that combined EPR and UV/VIS-DRS measurements are powerful tools for elucidating the nature of coexisting Fe species formed in the Fe-ZSM-5 materials investigated. The new structural data have been discussed with regard to the catalytic properties of the materials in the selective catalytic reduction of NO by isobutane or NH_3.

In the materials prepared, three different isolated sites have been identified by EPR spectroscopy, which have been assigned to Fe^{3+} in tetrahedral ($g' \approx 4.3$) and higher coordination ($g' \approx 6$), and to Fe^{3+} in a highly symmetric environment ($g' \approx 2$). The latter has been observed only in the sample with the lowest Fe content, A(MR) at low temperatures. In samples with higher Fe contents an intense signal of aggregated iron oxide species appears at the same g value of 2. UV/VIS-DRS differentiates between isolated Fe^{3+} sites, the coordination of which cannot be distinguished,

small (oligomeric) Fe oxide clusters, and large Fe oxide aggregates. The degree of aggregation and the order of the aggregates can also be studied by temperature-dependent EPR measurements where it is reflected in increasing intensity of the cluster signal due to breakdown of the antiferromagnetic coupling. Based on these assignments, the following conclusions could be derived:

All preparations (including the mechanochemical route) lead to the coexistence of different iron species. In all cases, isolated Fe sites are found, which are predominant after the mechanochemical route (which leads to low Fe content), but minority species with the other preparations. In the CVD preparation, clustered species occur already after the washing step, but their quantity and size increase strongly during calcination, with low gradients of temperature rise resulting in higher Fe dispersions. Intense washing of the material after the CVD step also favors higher Fe dispersion but does not prevent clustering. With a matrix of low density of Brønsted sites but high defect density, a low Fe dispersion before calcination was transformed into a highly disperse (but still largely clustered) Fe phase, probably due to the internal defects providing additional aggregation nuclei. Calcination leads also to a significant change in the coordination sphere of isolated Fe ions, which might be caused by a condensation of two charge-balancing OH groups to an O^{2-} ligand ($Fe(OH)_2{}^+ \rightarrow FeO^+$). The rehydration of the calcined state is slow at room temperature.

Comparison of the distribution of species detected by UV/VIS spectroscopy with activity trends in NH_3-SCR suggests that different entities (isolated sites, oligomers, probably also the surface of particles) participate in this reaction. The acidity of the zeolite is of minor importance with catalysts that contain clustered entities. For isobutane-SCR, the participation of isolated sites is suggested by the remarkable performance of a catalyst that is almost void of clustered entities. A participation of isolated sites is also inferred from the observation that during the use of the catalysts in the SCR reaction on a timescale where no deactivation was noted, oligomeric clusters tend to aggregate and achieve a more perfect order while the amount of isolated sites remains constant. Among the isolated sites, one (at $g' \approx 4.3$) appears to be insensitive to influences from the gas phase. Possible candidates for the active site are the signals at $g' \approx 6$ and $g' \approx 2$ (isolated species), where the latter is difficult to observe. The observation that nonselective oxidation of the reductant (isobutane or NH_3) starts at higher temperatures with a catalyst of low content of clustered species suggests that aggregates favor this undesired reaction.

Acknowledgment

We thank the Deutsche Forschungsgemeinschaft (DFG) for financial support (Grants Br 1380/7-1 and Gr 1447/7-1).

References

[1] G.I. Panov, G.A. Sheveleva, A.S. Kharitonov, V.N. Romannikov, L.A. Vostrikova, Appl. Catal. A 82 (1992) 31.
[2] A. Ribera, I.W.C.E. Arends, S. de Vries, J. Perez-Ramirez, R. Sheldon, J. Catal. 195 (2000) 287.
[3] J. Perez-Ramirez, F. Kapteijn, G. Mul, X. Xu, J.A. Moulijn, Catal. Today 76 (2002) 55.
[4] A.-Z. Ma, W. Grünert, Chem. Commun. (1999) 71.
[5] X. Feng, W.K. Hall, Catal. Lett. 41 (1996) 45.
[6] H.-Y. Chen, W.M.H. Sachtler, Catal. Today 42 (1998) 73.
[7] R.Q. Long, R.T. Yang, Catal. Lett. 74 (2001) 201.
[8] G. Berlier, G. Spoto, S. Bordiga, G. Ricchiardi, P. Fisicaro, A. Zecchina, I. Rossetti, E. Selli, L. Forni, E. Giamello, C. Lamberti, J. Catal. 208 (2002) 64.
[9] A.A. Battiston, J.H. Bitter, D.C. Koningsberger, J. Catal. 218 (2003) 163.
[10] F. Heinrich, C. Schmidt, E. Löffler, M. Menzel, W. Grünert, J. Catal. 212 (2002) 157.
[11] E.J.M. Hensen, Q. Zhu, M.M.R.M. Hendrix, A.R. Overweg, P.J. Kooyman, M.V. Sychev, R.A. van Santen, J. Catal. 221 (2004) 560.
[12] R.Q. Long, R.T. Yang, J. Am. Chem. Soc. 121 (1999) 5595.
[13] Q. Sun, Z.-X. Gao, H.-Y. Chen, W.M.H. Sachtler, J. Catal. 201 (2001) 88.
[14] A.A. Battiston, J.H. Bitter, D.C. Koningsberger, Catal. Lett. 66 (2000) 75.
[15] P. Marturano, L. Drozdova, A. Kogelbauer, R. Prins, J. Catal. 192 (2000) 236.
[16] J. Jia, Q. Sun, B. Wen, L.X. Chen, W.M.H. Sachtler, Catal. Lett. 82 (2002) 7.
[17] A.A. Battiston, J.H. Bitter, F.M.F. de Groot, A.R. Overweg, O. Stephan, J.A. van Bokhoven, P.J. Kooyman, C. van der Spek, G. Vanko, D.C. Koningsberger, J. Catal. 213 (2003) 251.
[18] R. Joyner, M. Stockenhuber, J. Phys. Chem. B 103 (1999) 5963.
[19] Z. Sobalik, A. Vondrova, Z. Tvaruskova, B. Wichterlova, Catal. Today 75 (2002) 347.
[20] F. Heinrich, C. Schmidt, E. Löffler, W. Grünert, Catal. Commun. 2 (2000) 317.
[21] H.-Y. Chen, El-M. El-Malki, X. Wang, R.A. van Santen, W.M.H. Sachtler, J. Mol. Catal. A: Chem. 162 (2000) 159.
[22] A. Brückner, R. Lück, W. Wieker, B. Fahlke, H. Mehner, Zeolites 12 (1992) 380.
[23] D. Goldfarb, M. Bernardo, K.G. Strohmaier, D.E.W. Vaughan, H. Thomann, J. Am. Chem. Soc. 116 (1994) 6344.
[24] A. Brückner, U. Lohse, H. Mehner, Micropor. Mesopor. Mater. 20 (1998) 207.
[25] A.V. Kucherov, C.N. Montreuil, T.N. Kucherova, M. Shelef, Catal. Lett. 56 (1998) 173.
[26] A. Brückner, G.-U. Wolf, M. Meisel, R. Stösser, H. Mehner, F. Majunke, M. Baerns, J. Catal. 154 (1995) 11.
[27] S. Bordiga, R. Buzzoni, F. Geobaldo, C. Lamberti, E. Giamello, A. Zecchina, G. Leofanti, G. Petrini, G. Tozzola, G. Vlaic, J. Catal. 158 (1996) 486.
[28] J.H. Bitter, A.A. Battiston, S. van Donk, K.P. de Jong, D.C. Koningsberger, Micropor. Mesopor. Mater. 64 (2003) 175.
[29] A. Brückner, B. Kubias, B. Lücke, Catal. Today 32 (1996) 215.
[30] P. Wenquin, Q. Shilun, K. Zhiyun, P. Shaoyi, Stud. Surf. Sci. Catal. 49 (1989) 281.
[31] A.F. Ojo, J. Dwyer, R.V. Parish, Stud. Surf. Sci. Catal. 49 (1989) 227.
[32] R. Aasa, J. Chem. Phys. 52 (1983) 3919.
[33] B.G. Fox, J.D. Lipscomb, in: C.C. Reddy, G.A. Hamilton, K.M. Madyastha (Eds.), Biological Oxidation Systems, vol. 1, Academic Press, San Diego, CA, 1990, p. 367.
[34] H.H. Tippins, Phys. Rev. B 1 (1970) 126.
[35] G. Lehmann, Z. Phys. Chem. Neue Folge 72 (1970) 279.
[36] X. Gao, I.E. Wachs, J. Phys. Chem. B 104 (2000) 1261.

[37] P. Marturano, L. Drozdova, D. Pirngruber, A. Kogelbauer, R. Prins, Phys. Chem. Chem. Phys. 3 (2001) 5585.
[38] J. Pérez-Ramirez, M. Santhosh Kumar, A. Brückner, J. Catal. 223 (2004) 13.
[39] M. Santhosh Kumar, M. Schwidder, W. Grünert, U. Bentrup, A. Brückner, in: 18th North American Catalysis Society Meeting, June 1–6, 2003, Cancun, Mexico, 2003, p. 4, Book of abstracts.
[40] A.V. Kucherov, C.N. Montreuil, T.N. Kucherova, M. Shelef, Catal. Lett. 56 (1998) 173.
[41] A.M. Volodin, V.I. Sobolev, G.M. Zhidomirov, Kinet. Catal. 39 (1998) 775.
[42] P. Kubánek, B. Wichterlová, Z. Sobalík, J. Catal. 211 (2002) 109.
[43] J. Dědeček, D. Kaucký, B. Wichterlová, Micropor. Mesopor. Mater. 35–36 (2000) 483.